Acta Polytechnica **62**(3):370–385, 2022
https://doi.org/10.14311/AP.2022.62.0370

Published by the Czech Technical University in Prague

EXPERIMENTAL AND SIMULATION STUDY OF CO_2 BREAKTHROUGH CURVES IN A FIXED-BED ADSORPTION PROCESS

Marek Nedoma[a,*], Marek Staf[b], Jan Hrdlička[a]

[a] *Czech Technical University in Prague, Faculty of Mechanical Engineering, Department of Energy Engineering, Technická 1902/4, 160 00 Prague 6, Czech Republic*

[b] *University of Chemistry and Technology, Department of Gaseous and Solid Fuels and Air Protection, Technická 5, 166 28 Prague 6, Czech Republic*

[*] corresponding author: marek.nedoma@fs.cvut.cz

Abstract.

This paper focuses on the laboratory experiments of low-temperature adsorption of CO_2 at elevated pressure and on the validation of our mathematical model with the data obtained. The numerical approach uses fitting of adsorption isotherm parameters and sensitivity analysis of parameters influencing the breakthrough curve shape and onset time. We first evaluate the results of breakthrough experiments for zeolite 13X. Then, we use the results obtained to design a dynamic mathematical model to predict the breakthrough curve profile. Experimental results show that zeolite 13X possesses high adsorption capacities (over 10 % of its weight at adsorption temperatures of 293 K and below), as expected. The mathematical simulation was accurate at predicting the breakthrough onset time; however, this prediction accuracy declined with the outlet CO_2 concentration exceeding 75 %, which is discussed. The sensitivity analysis indicated that the choice of different estimates of mass transport and bed porosity, as well as the choice of numerical scheme, can lead to a more accurate prediction, but the same set of parameters is not suitable for all process conditions.

Keywords: Adsorption, breakthrough experiment, CO_2 capture, mathematical modeling, sensitivity analysis.

1. Introduction

A gradual increase in burning fossil fuels emitting primarily CO_2 to the atmosphere has been considered as one of the reasons for steadily warming our planet over the past several decades. Carbon dioxide is a minor contributor to global warming or climate change among greenhouse gases [1], but EU climate policy has unanimously agreed through the Green Deal on targets to reduce CO_2 emissions and to phase out fossil fuels production, while supporting subsidies for non-carbon emitting alternatives [2].

Post-combustion technologies represent a group of non-carbon methods to capture CO_2 from an off-gas downstream of the original plant. Conventional methods are CO_2 scrubbing (e.g., using amine or ammonia solvents), adsorption, and membrane separation [3]. Apart from the principle of CO_2 separation itself, these technologies differ in the field of application where their deployment is the most efficient [4, 5]. Hence, a combination of them is another alternative, however, technically complicated [6]. The amine scrubbing for CO_2 capture is currently operating on a large scale; trade-offs are associated with energy intensive regeneration, toxicity, and instability of solvents [7]. Polymeric membranes generally suffer from expensive materials, laboratory equipment, and manufacturing, which prevents rapid development [8]. The adsorption phenomenon is based on a simple physical principle, however, there are challenges to be overcome, e.g., improvement of adsorption materials, large pressure drops in packed bed, and technical aspects of heat-induced desorption.

1.1. CO_2 capture by adsorption

In the adsorption system, emphasis must be placed on two key aspects: i) the technology and ii) the adsorbent [9].

In terms of technological aspects, the main emphasis should be put on the desorption method and on the bed configuration [10]; the choice of process parameters during adsorption, temperature and pressure can influence the working capacity [11] or the effect of adsorbing water if present in the flue gas [12]. The desorption of the adsorbent can be performed by alternating pressure (pressure- or vacuum-swing cycles), temperature (temperature-swing cycles), or by its combination, i.e., coupling cycles [9]. Pressure-swing systems take place in a fixed-bed reactor, whereas moving-bed, rotary-bed, or fluidised bed reactors are often used in a combination with temperature-swings due to a significantly higher heat transfer rate [10].

The choice of the desorption method and its operating conditions is influenced by the process economy, cycle duration, adsorbent life span (cyclic stability) and working capacity, etc., and by the demands for quality

(purity) and quantity (productivity) of the captured CO_2. The PSA method is well-recognized in industry, for example, in air separation and hydrogen production. However, for the post-combustion CO_2 capture, the atmospheric (desorption) pressure is insufficient to obtain high purity CO_2 and the energy consumption associated with gas pressurisation increases rapidly with volumetric flow. VSA cycles are a method of choice by many, for the simplicity and reliability of fixed-bed operation, and a favourable performance of readily available activated carbon or zeolite-based adsorbents; however, producing high purity CO_2 may require inclusion of a second desorption stage. Fixed-bed column sizing, resulting in large column trains for large flue gas throughput, may be overcome by TSA cycles. These cycles have received increasing attention due to the proliferation of research in alternative bed concepts enabling faster cycling by better heat propagation or processing of larger amounts of gas in a single column, as in the case of rotary adsorbers [3, 13]. Furthermore, temperature swings allow to operate on a wider range of working capacities, for example, of metal-organic frameworks (MOFs) [14]. Generally, adsorbents with higher working capacities are better suited for pressure-swing-based cycles, whereas TSA can exploit the potential of high working capacities better, achieving a lower energy consumption relative to sorbent inventory [15, 16]. Solving the long TSA cycle times decreasing productivity, among other factors, is still a challenge. Therefore, carefully combining pressure- and temperature-swings becomes attractive [13].

An adsorbent is a solid substance (carbonaceous or non-carbonaceous) that should possess high CO_2 sorption capacity, high CO_2 selectivity, good kinetics, mechanical strength, and so on, while being inexpensive to manufacture [17].

The classification of adsorbent usually has to be known prior to the technology. It can be performed experimentally in several ways, most commonly: breakthrough experiments, volumetric analysis, thermogravimetric analysis, or zero-length column technique [18]. The selection of suitable adsorbents is followed by a process analysis. Its performance is evaluated by a theoretical calculation or measurement of CO_2 purity after desorption, adsorbent recovery, CO_2 productivity, and energy consumption of the process. These parameters are typically related to each other [19]. Productivity is related to the management of captured CO_2, e.g., storage or utilisation (in most cases, 95 % purity is required [20]). Energy consumption is of great importance in the industrial sector [21]. An experimental acquisition of these parameters is the most valuable, but generally expensive and time-consuming. The prevailing trend is to use a mathematical simulation to predict the physical properties of certain adsorbents (typically, finely tuned MOFs by so-called "adsorbent screening" [22, 23]), as well as the process performance in a fraction of the time [24]. Once verified by experimental data, the mathematical model can be applied to any system with a similar configuration, allowing to use different parameters or materials.

In this paper, we address an experimental characterisation of CO_2 adsorbents in a fixed bed laboratory apparatus and validation of a mathematical model using the obtained results. The model was designed in accordance with the ongoing process in the apparatus. It is used to predict the shape of the breakthrough curve, obtained from the experiments, and subsequently subjected to a sensitivity analysis.

2. Materials and Methods

2.1. Materials

In this work, we have selected a commercial sample of porous non-polar adsorbent without any further modifications, molecular sieve 13X (*Merck - Sigma-Aldrich*, Germany), for the CO_2 adsorption experiments. The adsorbent particles with homogeneous structure had a regular spherical shape and smooth surface. Their diameter ranged from 1.9 to 2.1 mm with a volume of $2.84 - 3.46$ mm^3; other characteristics are summarised in Table 1.

2.2. Experimental setup

An experimental apparatus for the adsorption experiments was built on the basis of a former high-temperature fluidized bed system [25]. Details are listed in Table 1 and Figure 1.

The apparatus is composed of the gas distribution and flow control systems, the adsorption column and humidifier, the climate chamber with programmable temperature controller, and the analytical terminal. The front and top views (same measuring scale) are shown in Figure 3. Figure 4 shows a glazed chamber after the apparatus is placed inside the climate chamber, which ensures the desired temperature of the entire system.

The core of the adsorption apparatus is a cylindrical stainless steel adsorption column, in which the adsorbent is placed.

The gas mixture simulating the pre-purified flue gas (i.e., undergoing a denitrification, desulphurisation, and eventual drying since it is virtually impossible to separate CO_2 from untreated flue gas with a single layer of adsorbent [26]) is supplied from a gas cylinder. After passing through the flow controller, the gas is split into two streams by a manual ball valve switch, and can be fed directly into the adsorber or into the spectrometer. This principle is used to evaluate the adsorption capacity. Before entering the adsorber, the gas stream is split again. The first path leads to humidifiers capable of achieving a relative humidity (RH) of $70 - 85$ % at a given temperature and pressure. The second path, used in this study, bypasses the humidifier. The gas passes through the adsorber from the top to the bottom. The gas leaving

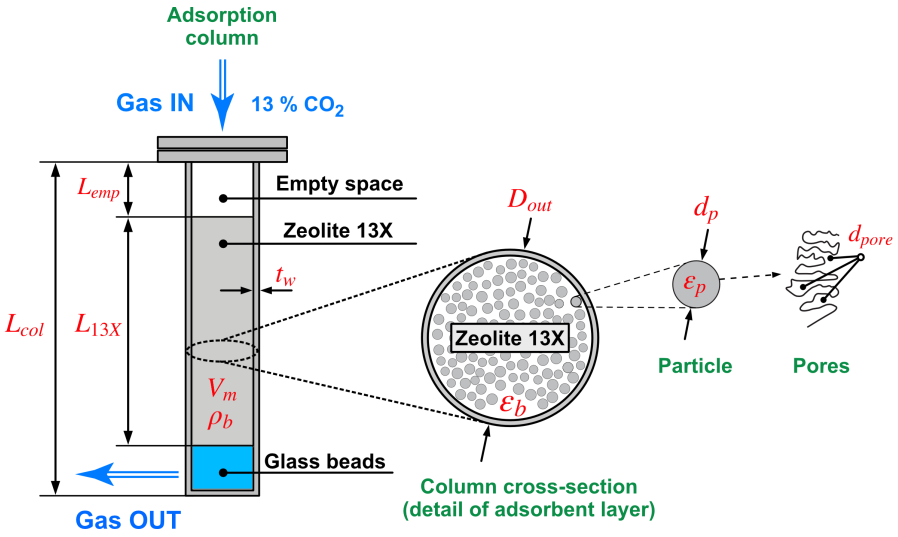

FIGURE 1. Adsorption column scheme.

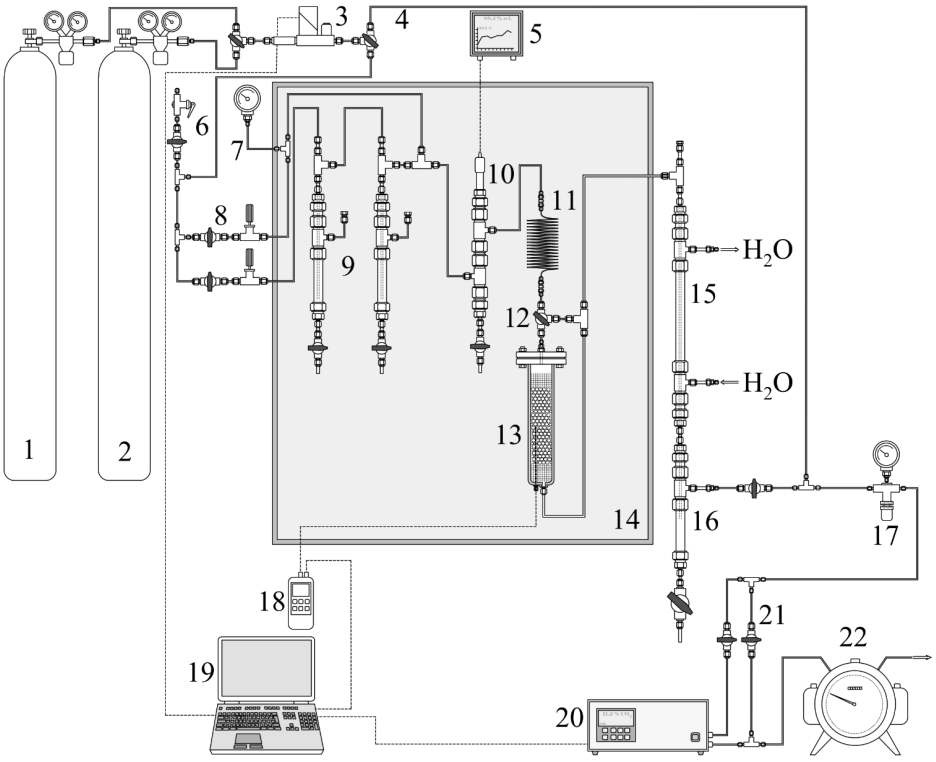

FIGURE 2. Scheme of the adsorption apparatus: 1, 2 - gas cylinders, 3 - mass flow meter with controller, 4 - three-way valve of the main bypass, 5 - hygrometer display unit, 6 - safety valve, 7 - control manometer, 8 ball and needle valves of humidifier, 9 - pair of humidifiers, 10 - hygrometer pressure sump, 11 - spiral heat exchanger, 12 - three-way valve of the adsorber internal bypass, 13 - adsorber, 14 - climate chamber, 15 - liquid cooler, 16 - condensate sump, 17 - back pressure regulator, 18 - thermometer / data-logger, 19 - PC for data collection and process setting, 20 - infrared spectrometer, 21 - spectrometer bypass setting, 22 - drum-type gas meter.

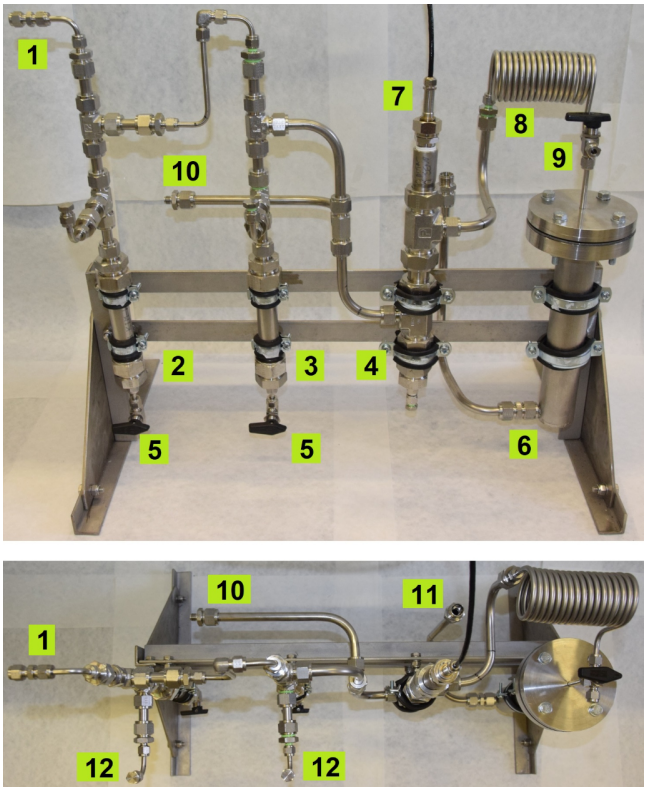

FIGURE 3. Adsorber and humidifier assembly: 1 - gas inlet of the humidifier, 2, 3 - humidifier chambers, 4 - hygrometer pressure sump, 5 - water discharge, 6 - adsorber, 7 - hygrometer probe, 8 - heat exchanger, 9 - three-way valve of the adsorber internal bypass, 10 - dry gas path inlet 11 - adsorber outlet, 12 - water inlet regulator (humidifier wetting).

FIGURE 4. Outside view of the testing apparatus: **A)** 1 - glazed chamber, 2 - adsorber assembly in the climate chamber, 3 - PC (data collection and process control), 4 - side chamber passage of pipes and cables, 5 - liquid cooler, 6 - thermometer with data-logger, 7 - infrared spectrometer, 8 -mass flow meter with controller, 9 - safety valve, 10 - drum-type gas meter, 11 - condensate sump; **B)** climate chamber with the assembled adsorption apparatus.

Adsorption column - Fixed bed	
Material	Stainless Steel
Inner column length, L_{col}	0.26 m
Empty space length, L_{emp}	0.08 m
Inert bed length, L_{gb}	$0.019 - 0.025$ m
Adsorbent bed length, L_{13X}	$0.155 - 0.161$ m
Inner diameter, D_{in}	0.04 m
Wall thickness, t_w	0.002 m
Adsorbent - Zeolite 13X	
Material	Molecular sieve 13X, Sigma Alrich
Material volume, V_m	$195 - 202\,\mathrm{cm}^3$
Material weight, m_m	$0.1425 - 0.1435$ kg
Bulk density, ρ_b	$710 - 730\,\mathrm{kg/m}^3$
Bed porosity, ε_b	0.373^*
Particles shape	Homogenous spheres
Particle diameter, d_p	$1.90 - 2.10$ mm
Particle volume, V_p	$2.84 - 3.46\,\mathrm{mm}^3$

Estimated using Equation 2.

TABLE 1. Apparatus dimensions, physical properties of the adsorbent material (Zeolite 13X) and the fixed-bed.

the adsorber and the climate chamber is cooled in a liquid bath. Any excess moisture is condensed, and the gas pressure is reduced to atmospheric level. At the outlet of the apparatus, the gas enters an infrared (IR) spectrometer *Ultramat 23 IR* and then a drum-type gas meter. Monitoring of the adsorption and desorption is carried out by an online analysis of the gas flowing through the apparatus. The method of sorption rate evaluation is based on the comparison of the adsorptive content in the gas at the adsorption column's inlet and outlet. A view of the apparatus in operation is shown in Figure 4.

2.3. Breakthrough experiments

The breakthrough experiment is performed under dynamic conditions with a constant flow rate at the inlet. The investigated gas mixture contains a known concentration of the adsorptive. From the obtained breakthrough curves, other physical parameters, such as adsorption rate, separation efficiency under given conditions, and specific consumption of sorbent can be evaluated.

The actual measurement of one cycle consisting of adsorption and desorption is performed as follows:

1. **Regeneration**: the adsorbent is first dried to a constant weight and then placed into the adsorber. Nitrogen at a flow rate of 2 dm^3/min is introduced into the adsorber, and the chamber temperature is set to 393 K. After a complete regeneration, indicated by the IC spectrometer, an adsorption step begins.
2. **Adsorption (breakthrough experiment)**: initially, a stream of nitrogen passes through the adsorber, which is set to the working overpressure (2 or 5 bar). The temperature in the chamber is reduced to the desired adsorption temperature, which was set to 283, 293, 303 or 313 K. After the temperature in the adsorbent layer has stabilised, the inert gas is changed to the simulated flue gas. It consists of 13 vol. % of CO_2 balanced by synthetic air. The adsorption phase ends when the CO_2 concentrations at the inlet and outlet of the adsorber are equal. This state indicates an adsorption equilibrium when the adsorption capacity of CO_2 at a given pressure, q_i^* $\left[\mathrm{g}_{\mathrm{CO_2}}/\mathrm{g}_{\mathrm{dry\ adsorbent}}\right]$, is reached. Blank experiments have been carried out using inert material (glass beads of the same total volume as the real sample) prior to CO_2 adsorption. The blank curves are shown in Figure 5.
3. **Desorption**: the desorption was carried out at atmospheric pressure and elevated temperature (i.e., PTSA cycle). Once the CO_2 is released from the solid phase, the column is purified by N_2 or any other non-reactive gas (if CO_2 is used as a purifying gas, which is a common practice in the industry to maintain maximum purity of the product, it is not possible to use the IR spectrometer).

2.4. Mathematical modeling of breakthrough data

The breakthrough experiment was described by a one-dimensional plug-flow mathematical model in a packed-bed with the following assumptions:

1. The gas is a binary mixture of CO_2 and N_2 and behaves according to the ideal gas law (O_2, contained in the synthetic air, has similar adsorption characteristics as N_2, because its affinity towards Zeolite 13X is more-or-less equal to the affinity of N_2, thus both gases adsorb weakly [27]; the literature generally provides expressions for binary diffusion, the

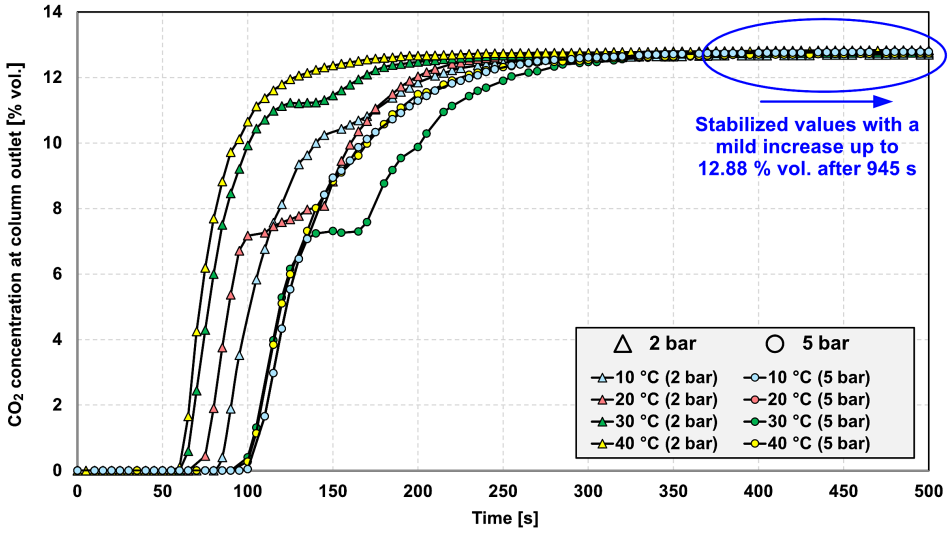

FIGURE 5. Blank experiments performed prior to each measurement; operating conditions: T = 10 - 40 °C, P = 2, 5 bar. The time interval is shortened from about 1800 s to 500 s, when the CO_2 concentrations at the outlet are almost stable.

diffusion of gas mixtures with more components is less accurately predictable [28].).

2. The system is isothermal (without generation of adsorption heat) and adiabatic (heat loss to the outside environment is not considered).
3. The system is radially homogeneous without the occurrence of concentration, diffusion, and temperature radial gradients.
4. The change in kinetic and potential energies is negligible.
5. The physical properties of the gas mixture, such as adsorption enthalpy, density, diffusion coefficients, specific heat capacity, and dynamic viscosity, are constant.
6. The physical properties of the adsorbent as well as the bed porosity are uniform.
7. The mass transfer rate between the solid and gas phases is described by the linear driving force (LDF) model.
8. The adsorbent is fully regenerated at the beginning.
9. The pressure drop is negligible, and the interstitial velocity of the gas is assumed to be constant.

The ongoing adsorption process in our experimental setup differs from the real adsorption systems by the placement of the apparatus and by its configuration. The adsorption column is placed inside a thermally insulated chamber, which makes it possible to reach isothermal conditions after a few minutes from the start of the process. Normally, the temperature varies continuously with respect to the generated adsorption heat and the volumetric flow having a higher overall effect on the adsorption phase such as the propagation of the concentration front. By assuming isothermal conditions (assumption 2), the prediction error is thus reduced; we discuss its effect within the following Section. Assumptions 1, 3, 5, 6 and 7 simplify the phenomena, but their application is proven to be sufficient [29]. Assumption 8 characterizes the breakthrough experiment [30], or the first cycle in the adsorption systems, because subsequent cycles do not allow full adsorbent regeneration after the desorption, leading to a cyclic deterioration of the adsorption capacity. Adsorption of gases causes a different volumetric flow, i.e., velocity of the purified gas at the column outlet. However, due to the nearly constant pressure and the small amount of strongly adsorbable components, this effect is less significant [31]. The change in volumetric flow, which we measured experimentally and which will be discussed later, occurs only when CO_2 is detected at the outlet (adsorbent is, at this time, almost saturated) and dilutes the purified gas, that is, N_2.

Based on the assumptions, the system is described by two governing Equations (1) and (4). The mass balance equation for component i in the gas phase assumes advection-diffusion plug-flow and is defined as follows:

$$\frac{\partial c_i}{\partial t} = \frac{\partial}{\partial z}\left(D_{\mathrm{ax}}\frac{\partial c_i}{\partial z}\right) - u\frac{\partial c_i}{\partial z} - \rho_p\left(\frac{1-\varepsilon_b}{\varepsilon_b}\right)\frac{\partial q_i}{\partial t} \quad (1)$$

Where $c_i = (y_i P)/(RT)$ is the concentration in the gas phase $\left[\mathrm{mol/m^3}\right]$, u is the interstitial velocity [m/s], ρ_p is the adsorbent particle density $\left[\mathrm{kg/m^3}\right]$, and ε_b is the bed porosity. Bed porosity was calculated using a correlation proposed by [32], which takes into account the column dimensions and the mean particle size of the adsorbent d_p [m]:

$$\varepsilon_b \;=\; 0.373 + 0.917 \exp\left(-0.824\,\frac{D_{in}}{d_p}\right) \qquad (2)$$

An alternative would be a comparison of the gas flow rate before the gas enters the adsorbent and of the gas flow rate inside the adsorbent. In the experiments, this measurement was obtained only for a single experimental case, 283 K and 5 bar, and therefore, using an experimentally verified formula is more rigorous. This approach was also used for the determination of interstitial velocity.

The D_{ax} represents the axial dispersion coefficient of the gas mixture $\left[\mathrm{m}^2/\mathrm{s}\right]$, which is dominant in the axial direction at higher Reynolds numbers ($\mathrm{Re_p} > 10$) [33]. Radial gradients are neglected. A correlation of Edwards and Richardson (1970) incorporating Wicke's (1973) approximation of coefficient γ and Bischoff's (1969) expression of coefficient β was used. The calculation of the D_{ax} is described in detail in [30] for a packed-bed adsorption of CO_2:

$$D_{\mathrm{ax}} \;=\; \gamma \cdot D_{M,\,CO_2-N_2} \;+\; \frac{\mathrm{Pe}_\infty^{-1}\,(u \cdot d_p)}{1 \;+\; \dfrac{\beta \cdot \gamma \cdot D_{M,\,CO_2-N_2}}{u \cdot d_p}} \qquad (3)$$

The advantage of this equation is that it accounts for the size of the adsorbent particles by a function of limiting value of Péclet number, Pe_∞, which was calculated by [34] as $Pe_\infty = 6.7\,d_p$ for particle size of the adsorbent lesser than 0.25 cm.

The last term in Equation (1), a source term, represents a mass transfer of the adsorbate in the solid phase and is simplified by the LDF model [35] assuming that the mass accumulation of a component i in the adsorbent is proportional to the difference between the amount adsorbed at equilibrium q_i^* $\left[\mathrm{mol}/\mathrm{m}^3\right]$ (given by the equilibrium adsorption capacity of the adsorbent measured during the breakthrough experiments) and the mean value of the amount adsorbed in the adsorbent particle q_i $\left[\mathrm{mol}/\mathrm{m}^3\right]$:

$$\frac{\partial q_i}{\partial t} \;=\; k_i\,(q_i^* \;-\; q_i) \qquad (4)$$

The mass transfer coefficient of component i, k_i [1/s], is simplified to the resistance of mass transport by diffusion in macropores, which usually dominates in commercial zeolites that are purposely made to minimise micropore diffusion and depends on the r_p^2/d_p ratio. The resistance to gas permeation through the film layer around the adsorbent is usually insignificant [36]:

$$k_i \;=\; \frac{15\,D_{\mathrm{eff}}}{r_p^2} \cdot \frac{c_{\mathrm{in},\,i}}{\rho_p \cdot q^*_{\mathrm{in},\,i}} \qquad (5)$$

Where r_p is the adsorbent particle diameter [m], D_{eff} is an effective value of the diffusion coefficient $\left[\mathrm{m}^2/\mathrm{s}\right]$ and $c_{\mathrm{in},\,i}\,/q^*_{\mathrm{in},\,i}$ represents a dimensionless slope of the adsorption isotherm that must be used for adsorbent particles with homogeneous structure. Effective diffusion depends on the flow regime in the macropores, which is determined from the Knudsen number [37]. The diffusion transport in macropores in zeolites takes place in the transition area, where both mechanisms, Knudsen and molecular diffusions, play an equal role:

$$D_{\mathrm{eff}} \;=\; \frac{\varepsilon_p}{\tau}\left(\frac{1}{D_{M,\,CO_2-N_2}} \;+\; \frac{1}{D_K}\right)^{-1} \qquad (6)$$

A pore geometrical factor τ, tortuosity, ranges from approximately 2 to 3 in packed beds filled with a non-structured zeolite adsorbent [38], but a value of 3 was chosen [30]. The porosity of the adsorbent particle ε_p was calculated using both the estimated (ε_b) and the experimentally measured ($\rho_b,\ V_{\mathrm{pore}}$) values:

$$\varepsilon_p \;=\; \rho_p \cdot V_{\mathrm{pore}}, \qquad (7)$$

where ρ_p is the particle density $\left[\mathrm{kg}/\mathrm{m}^3\right]$ and V_{pore} is the volume of pores $\left[\mathrm{m}^3/\mathrm{kg}\right]$.

There are many correlations that can be applied to estimate the molecular diffusivity. An approximation by Fuller et al. (1969) was used, which, according to [28], provides high accuracy for the binary mixture of $CO_2 - N_2$:

$$D_{M,\,CO_2-N_2} \;=\; \frac{0.00143\,T^{\,1.75}}{P \cdot M_{CO_2-N_2}\left[\left(\sum \nu_{CO_2}\right)^{1/3} + \left(\sum \nu_{N_2}\right)^{1/3}\right]^2} \qquad (8)$$

Where P is the gas pressure [bar], T is the temperature [K], and ν is the molar volume of the gas phase $\left[\mathrm{m}^3/\mathrm{mol}\right]$. The Knudsen diffusivity of component i, D_K $\left[\mathrm{m}^2/\mathrm{s}\right]$, was approximated by the Derjaguin correlation [39]:

$$D_{K,\,i} \;=\; \frac{9}{13}\left(\frac{d_{\mathrm{pore}}}{3}\sqrt{\frac{8\,R\,T}{\pi \cdot M_i}}\right) \qquad (9)$$

Where d_{pore} is the pore diameter [m], R is the universal gas constant [J/ (mol.K)] and M_i is the molar weight of component i [kg/mol]. The overall Knudsen diffusion, D_K $\left[\mathrm{m}^2/\mathrm{s}\right]$, of gas mixture was calculated as resistances connected in parallel.

The system of governing equations with fixed initial and boundary conditions was differentiated with respect to the axial axis z and the time t to obtain the concentration of CO_2 and N_2 in the gas phase and the adsorption rate in the solid phase. The adsorption is a dynamic process accompanied by step change of concentration caused by the decomposition of the transport mechanism from purely convective to convection and diffusion once the gas enters the unsaturated empty bed, hence the Danckwers boundary condition $D_{\mathrm{ax}}\left(\partial c_i\,(t, 0^+)\,/\partial z\right) = u\left[c_i\,(t, 0^+) - c_{i,\,\mathrm{in}}\,(t, 0^+)\right]$ [40] for the column inlet was applied. A higher accuracy of approximation was achieved by using a higher

Surface characteristics	
BET surface area, S_{BET}	$511.65\ \mathrm{m^2/g}$
Total pore volume, V_{pore}	$3.317 \times 10^{-4}\ \mathrm{m^3/kg}$
Pore average diameter, d_{pore}	$3.33 \times 10^{-8}\ \mathrm{m}$
Breakthrough experiments	
Adsorption pressure, P	2, 5 bar
Adsorption temperature, T	283, 293, 303, 313 K
Volumetric flow, V	
→ 2 bar	$0.024 - 0.045\ \mathrm{m^3/h}$
→ 5 bar	$0.021 - 0.023\ \mathrm{m^3/h}$
CO_2 molar fraction, y_{CO_2}	0.13
Adsorption capacities, q^*	
→ 2 bar and 283, 293, 303, 313 K	0.1188, 0.1000, 0.0737, 0.0681 $\mathrm{g_{CO_2}/g_{sorbent}}$
→ 5 bar and 283, 293, 303, 313 K	0.1313, 0.1128, 0.0872, 0.0809 $\mathrm{g_{CO_2}/g_{sorbent}}$
Desorption pressure, P	1 bar
Desorption temperature, T	393 K

TABLE 2. Experimental results and model parameters.

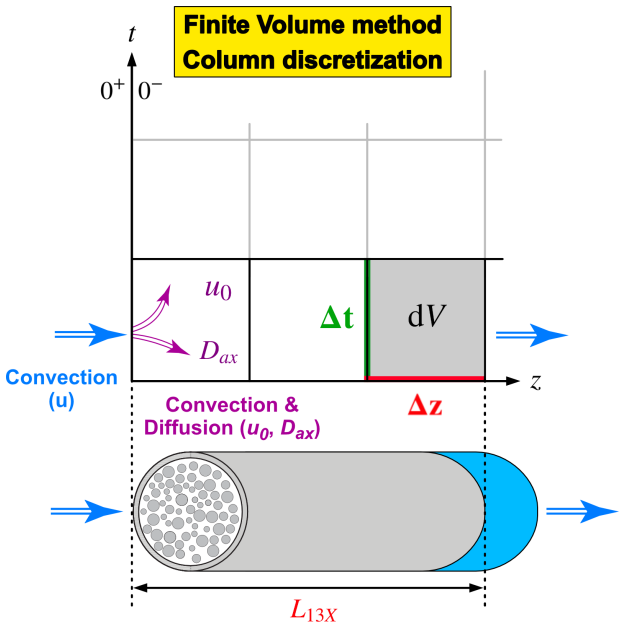

FIGURE 6. Schematic discretisation of the adsorption column using a finite volume method.

schemes with flux limiters recommended by [41] for a lumped kinetic model to ensure stability of the solution. A second-order TVD (total variation diminishing) explicit finite volume scheme was used, and equations were solved in MATLAB for the length step $\Delta z = 0.003\,\mathrm{m}$ and time step $\Delta t = 0.003\,\mathrm{s}$. The column discretisation into a series of control volumes $\mathrm{d}V$ along the axial axis z is shown in Figure 6. additional model parameters, which were obtained experimentally or by parameters estimation are specified in Table 2.

3. Results and discussion

3.1. Breakthrough experiments

The surface characteristics of the Zeolite 13X (BET surface area, S_{BET} $\left[\mathrm{m^2/kg}\right]$, and pore size distribution) were analyzed using a Coulter SA 3100 particle size analyzer. The measurement consisted of a pure nitrogen adsorption at 77 K, followed by determination of pore volumes from the obtained absorption isotherms. The results are listed in Table 2, together with the CO_2 adsorption capacities measured in the breakthrough experiments. The pore size distribution is shown in Figure 7.

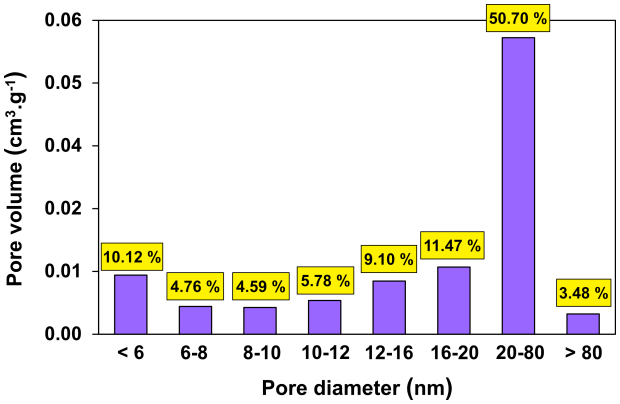

FIGURE 7. Pore size distribution.

BET analysis was also used to calculate the average size of the pores: $d_{\mathrm{pore}} = (4\,V_{\mathrm{pore}})\,/\,S_{\mathrm{BET}}$. Different mechanisms of mass transport in pores (pore size classification by IUPAC [42]) were not considered in diffusivities, and except for macropores ($> 50\,\mathrm{nm}$), all adsorbent pores were considered mesopores.

Each measurement of the breakthrough curve was carried out after 24 hours of desorption by degassing in an insulated reactor at 423 K.

A total of 5 cycles of adsorption and desorption at steady state were made for each temperature and pressure, as described in Section 2.3. The measured equilibrium adsorption capacities were averaged and summarised in the graph shown in Figure 8.

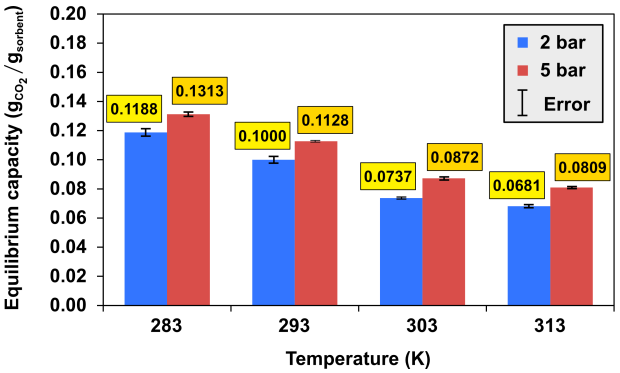

Figure 8. Adsorption capacities averages over cycles in each measurement.

A maximum variation for each individual adsorption pressure ranged from 0.97 % to 2.32 % at 2 bar, and 0.49 % to 1.20 % at 5 bar. The dependence of the magnitude of the error on the measurement conditions did not show a clear trend for adsorption temperature, but the average adsorption capacity varied more between cycles at the lower adsorption pressure, i.e., 2 bar. A possible explanation could be that higher pressures cause faster adsorption, as evidenced by the breakthrough curves measured at 5 bar (Figure 11). The adsorbate is, therefore, attracted by a greater force (van der Waals forces), which may result in a smaller deviation over a shorter period of time.

As expected, the commercial 13X molecular sieve sample showed the highest CO_2 adsorption capacities at high pressure and low temperature, that is, 0.1188 $g_{CO_2}/g_{sorbent}$ at 283 K and 2 bar and 0.1313 $g_{CO_2}/g_{sorbent}$ at 283 K and 5 bar. These conditions can be reached only when the water vapor is removed from the gas, which is a typical demand for zeolite-based adsorbents. In case the water vapor content is negligible or resistant adsorbent is used, lowering the flue gas temperature from 303 K to 293 K would improve the adsorption capacity of CO_2 the most. However, if the temperature of the flue gas containing a high amount of water vapor is around 303 K, it is due to consider adsorption at higher temperature, where the adsorption capacity is no longer significantly reduced, but the need for dehydration may be eliminated.

Once most of the adsorbent is saturated, we observed that the volumetric flow gradually increased appropriately to the amount of non-adsorbed CO_2 present. An almost linear dependence between both curves is not surprising (see Figure 9); however, when comparing the price of a CO_2 sensor and the difficulty of concentration sensing against sensing of a mass-flow rate, it begs the question of whether a similar idea could be interpreted into, for example, multi-column systems where mass-flow meters could serve as indicators of CO_2 concentration at each outlet, detecting the permitted amount of CO_2 in the off-gas. Especially in the industry, the requirement is aimed at process control and management rather than at measuring precision. However, knowing the information about the change in CO_2 concentration at the outlet, one can inversely predict the off-gas volumetric flow-rate and hence its velocity and pressure drop absolute variation. Further use of such information could also be replicated in the simulation to estimate, for example, the growth of axial dispersion in a system without pressure loss. However, the prediction error rate would require a deeper analysis.

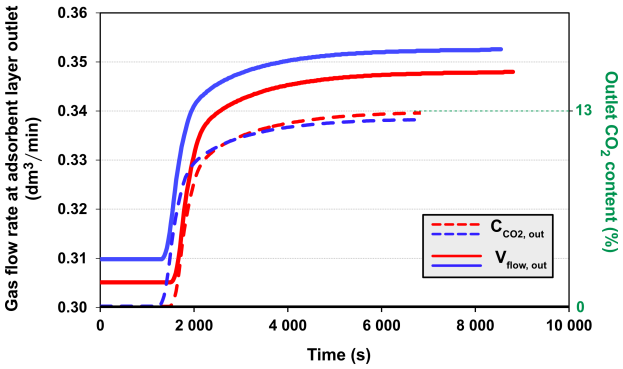

Figure 9. Experimentally measured values of volumetric flow and of CO_2 concentration at the column outlet. The curves shown have the highest deviation of values measured at 283 K and 5 bar.

3.2. Simulation results

The model parameters that were obtained by the adsorbent classification and breakthrough experiments or by using the aforementioned correlations are presented in Table 2, the rest of the input values can be found in Table 1.

The breakthrough curve modelling had to deal with incomplete experimental data, because the CO_2 adsorption isotherm was not measured. Its impact on the breakthrough curve is significant, as it influences the mass transfer rate coefficient representing the magnitude of the adsorption rate and defines the affinity of the adsorbate species towards the adsorbent (maximum adsorption amount at equilibrium was known). Generally, there are fewer experimental data available at higher pressures, and each of them usually differs in the sorbent used (for example, manufacturer, the Si/Al ratio, the framework structure, etc.). The interested reader is referred to, e.g., study by Hefti et al. [43] and summary within, or to the *NIST ARPA-E* [44] database currently containing 35 studies with CO_2 adsorption isotherms up to 5 bar. Due to the aforementioned diversity of adsorbent samples, making it difficult to replicate other data on the 13X sample tested in our study, we decided to follow the approach

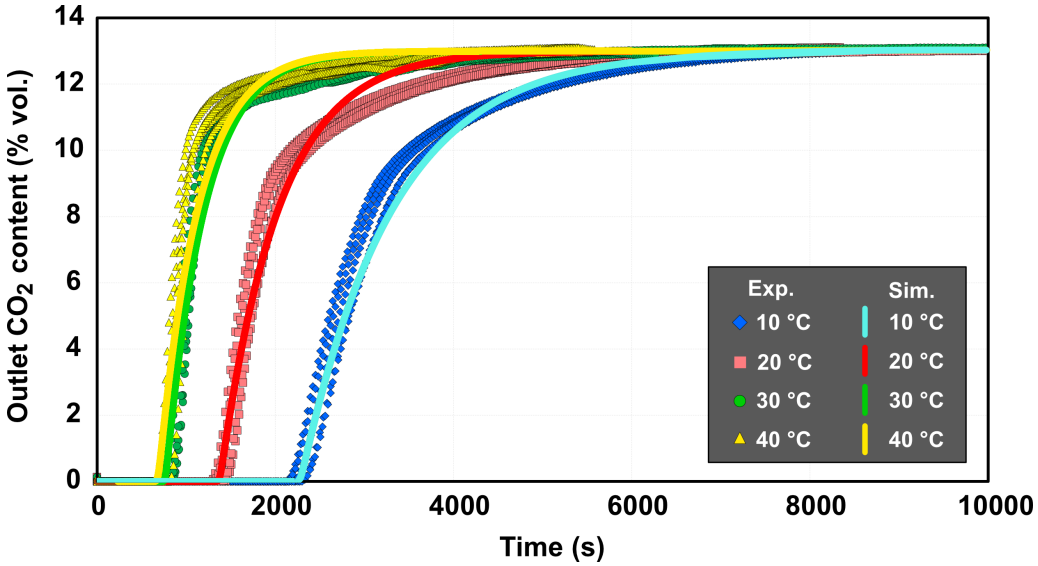

FIGURE 10. Comparison between the experimentally measured breakthrough curves and curves obtained by the simulation at 283, 293, 303 and 313 K, and 2 bar. *Note:* Exp. = Experiment; Sim. = Simulation; the curves obtained by the simulation are ploted in the black, and green, respectively, for the 30 °C.

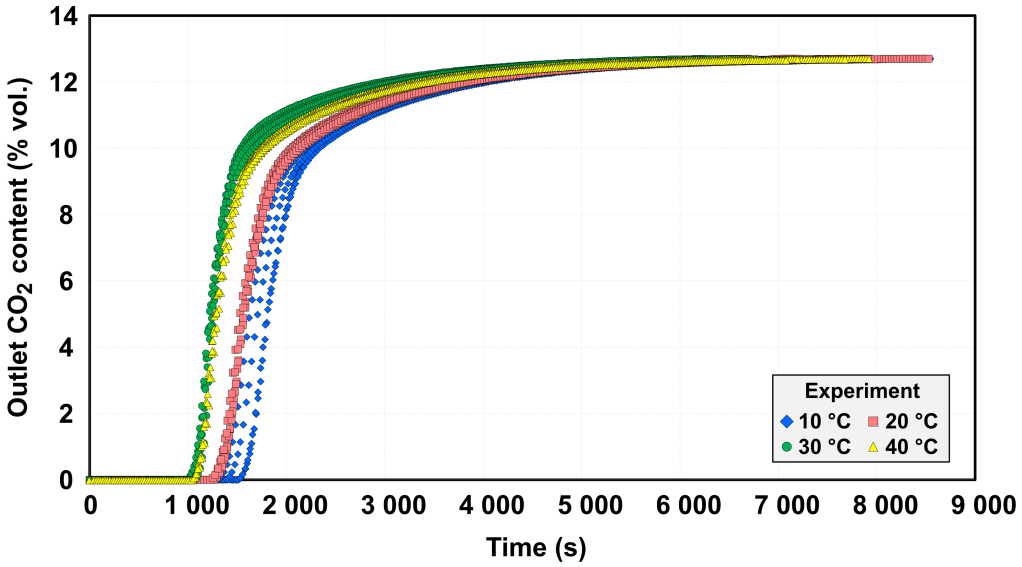

FIGURE 11. Experimentally measured breakthrough curves at 283, 293, 303 and 313 K, and 5 bar.

used by [45] and fit parameters of a single-site Langmuir isotherm:

$$q_i^* = \frac{q_{\text{sat}} \cdot b_i \cdot c_i}{1 + b_{\text{CO}_2} \cdot c_{\text{CO}_2} + b_{\text{N}_2} \cdot c_{\text{N}_2}} \qquad (10)$$

The use of the single-site Langmuir isotherm may look like a simplification because more complex models can better approximate the nonlinearity of CO_2 adsorption. For example, Bekhti et al. [46] compared 8 adsorption isotherm models for CO_2 on NaY zeolite up to 1 bar, and although the dual-site and the multi-site Langmuir isotherms had the smallest error, the single-site Langmuir isotherm was considered sufficient. We wanted to start with a simple model, which turned out to be sufficient even for higher pressures, despite the recommendation of Hefti et al. [43]. Using another model could raise the question of the number of fitting parameters, and therefore uncertainty, which is why we did not investigate other models. Such a comparison with the absence of the actual adsorption isotherm may be an interesting topic for further study.

We used a similar optimisation technique by changing the Langmuir equilibrium constant $b_{0,\,i}$ [m^3/mol], the internal energy ΔU_i [J/mol] (functions of an equilibrium constant b_i [m^3/mol]), while respecting the range of values for CO_2 and N_2 recommended by [45], and the maximum saturation capacity of the monolayer, q_{sat} [mol/kg]. The aim of this optimisation was to predict the breakthrough onset time by one-time adjustment of the adsorption isotherm within

the range of 5 experimentally measured isotherms at each of 4 cycles at 2 bar.

The fitting process was performed in MATLAB for 283 K. The best possible shape of the breakthrough curve was achieved by changing mostly the q_{sat}, $b_{0,\,CO_2}$ (ΔU_i remained constant, because of high sensitivity to the stability of the numerical solution in the region before the breakthrough occurred), and the flux limiter, which showed a high influence on the breakthrough curve slope. the following parameters were used:

$$\text{Fitting constraints} \begin{cases} q_{\mathrm{sat}} = 3.6 - 4.6 \\ b_{0,\,CO_2} = 2 - 2.5 \times 10^{-6} \\ \Delta U_{CO_2} = -35\,000 \\ \Delta U_{N_2} = -10\,000 \\ \text{Flux limiter: van Leer (1974)} \end{cases} \tag{11}$$

The "optimum solution" was obtained for $q_{\mathrm{sat}} = 3.7\,\mathrm{mol/m^3}$ and $b_{0,\,CO_2} = 2.1 \times 10^{-6}\,\mathrm{m^3/mol}$. The Langmuir constant for N_2 had a value of $b_{0,\,N_2} = 1.0 \times 10^{-6}\,\mathrm{m^3/mol}$. More details on calculating the single-site Langmuir adsorption parameters can be found in Pai et al. [45]. The breakthrough onset time correlated with a high degree of accuracy for other adsorption temperatures, 293, 303 and 313 K, while the fitting parameters remained constant. The region where the adsorption rate slows down as a result of high saturation of the adsorbent (the upper end of the curve) was accompanied by the highest deviation across the adsorption temperatures. An improvement was achieved by adapting the flux limiters used in the non-linear schemes, namely, van-Leer (1974) limiter instead of using the QUICK scheme.

Applying this approach, results can be generalised as follows:

- The prediction of the breakthrough onset time can be made with satisfying accuracy with 2 % maximum deviation from the experimental values (averaged over 5 cycles that were tested) across the range of adsorption temperatures. This also includes the area where the amount of 5 to 15 % of the inlet CO_2 concentration appears in the outlet, which would, in a real application, be an indication to terminate the adsorption process. The highest deviation was found for 283 K, where the predicted time for the occurrence of 15 % CO_2 from the inlet CO_2 concentration was 4.3 % (the deviation for 293 K was 0.2 %).
- To accurately predict the adsorbent utilisation efficiency (indicated by the slope of the breakthrough curve across its entire length) requires a deeper analysis of the parameters estimation and of the chosen numerical scheme. There is a relatively long-time interval before the breakthrough curve reaches its peak point because the change in the CO_2 concentration at the outlet decreases after approx. 75 % of the inlet CO_2 concentration. In our simulation, the deviation exceeded 10 % when the total amount of 90.2 % of CO_2 in the simulated gas (about 11.72 vol. % CO_2 relative to synthetic air) appeared at the outlet and the deviation continued to grow moderately. One of the possible explanations may be the negligence of the non-uniform generation of adsorption heat, i.e., exclusion of energy balance by assuming isothermal condition, or performing experiments in a rather small adsorption column (L_{col}/D_{in} ratio of 6.5), for which any change in temperature becomes more apparent relative to the breakthrough curve shape [47]. Results of Sircar (1983) [47] suggest a potentially higher correlation with our experimental data if the energy balance is accounted for (using temperature as a variable affecting both the adsorption rate and the equilibrium capacity results in a flattened curve plateau, i.e., long tail, until the feed concentration reaches the column outlet). Similar differences between isothermal and non-isothermal models using the LDF model for CO_2 adsorption were observed by [48]. On the contrary, Bollinini et al. (2012) [49] found the isothermal model relevant for lower flue gas velocities (higher velocities increase temperature); however, underlined the necessity of an appropriate value of the LDF mass transfer coefficient, k_i. Therefore, a follow-up study will be performed to confirm these claims as the objective of this study was to first verify the accuracy of predicting the breakthrough curve using a simple model.
  Theoretically, the CO_2 concentrations above, for example, 90 %, could be neglected, because they do not bring any significant improvement in the estimation of the adsorbent utilisation efficiency. However, using, e.g., a dimensionless factor π_1 proposed by [50] may be useful in this situation to ensure an "optimal" breakthrough curve steepness from the very beginning (recommended values of other criteria: Bi and π_2, proposed by the same authors, are usually satisfied for the fixed-bed adsorption). Furthermore, in a real process, it is unlikely that a similar amount of CO_2, at which our model showed the highest deviation, is allowed to be released in the atmosphere. Here, the inaccuracy of the isothermal model is significantly less important.

The experimental and simulation breakthrough curves are presented in Figure 10. The application of optimisation at 5 bar would be identical; hence Figure 11 shows only the experimental values.

3.3. Optimisation of the breakthrough curve prediction

Based on the differences between the experimental and simulation results, a sensitivity analysis was carried out to assess the accuracy of the prediction of the breakthrough onset time. Investigating the behaviour of the breakthrough curve in higher CO_2 outlet concentrations would be misleading in the sense that the

findings could not be directly applied to other temperatures as the breakthrough onset time. The approach was to assess parameters that are difficult to measure experimentally by nature, but the literature provides different ways of estimating them. For this purpose, a single breakthrough curve with the highest deviation (about 4 % from the original prediction) at 2 bar and 293 K was chosen, because it could represent a practical scenario in the CO_2 capture from the measured conditions.

First, it should be noted that the highest impact on the breakthrough onset time lies in the dimensions of the column and in the size of the adsorbent packing. For example, if the bed is fully filled with the zeolite 13X, achieving a breakthrough takes 51.6 % longer. Another obvious fact is that the breakthrough onset time decreases (and the curve becomes wider) with increasing volumetric flow. Second, the energy balance was not included in our model (discussed in Section 3.2), which partially limits the methodology of sensitivity analysis performed here. Sensitivity analysis was performed for 4 parameters:

- **Axial dispersion:** if the axial dispersion increases, the mixing of the gas molecules becomes more intensive, which results in an uneven adsorption and the breakthrough curve widens. Several correlations, chosen from [51], for the gas flow through the fixed bed packed with solid spherical particles were investigated. The values obtained were within the range of 3×10^{-5} m/s, and the breakthrough curve showed a negligible slope change. The highest difference was found between the correlations proposed by Edwards and Richardson (1968) and Wen-Fan (1975) with a difference of 1.62 % in the onset time.
- **Bed porosity**: it is proportional to the increase of the interstitial velocity, and therefore influences the axial dispersion. The estimation proposed by Ribeiro et al. [32] was in between the area of validity. Therefore, the calculation suggested by Dixon [52] for packed beds with regular spherical particles and a small ratio of the diameters of the column and the particles was analysed. The increase in the estimate of the bed porosity by approximately 14 % moved the results towards the experimentally obtained onset time by approx. 3.2 % and achieved the highest accuracy for the studied breakthrough curve (0.8 %; considering the average onset time for 2 bar, this change would also provide the best fit).
- **Mass transfer coefficient**: the mass transfer coefficient used in our model accounted for the transport resistance in macropores. As mentioned previously, commercial zeolites are made to minimise micropore diffusion; hence we have investigated whether the film layer slows down the gas penetration to a noticeable degree or whether the effect is negligible as suggested by [36]. An external mass transfer coefficient, k_f [m/s], with the [53] approximation of the Sherwood number, was included in the calculation of the overall mass transfer resistance. The obtained deviation of about 0.3 % confirmed the parameter's insignificance.
- **Molecular diffusion coefficient**: a less sensitive parameter. Any of the well-known expressions, e.g., Fuller et al. (1965), Wilke & Lee (1955) or Chapman-Enskog (1967), all contained in [28], provided almost identical results.

Lastly, the influence of the flux limiters was investigated. For this particular case, van-Leer (1974), Superbee (1986), and Koren (1993) achieved almost the same accuracy of 4 % (the highest of 3.8 % was achieved by the Superbee (1986) flux limiter). The highest difference between the numerical fluxes was observed for the less steep breakthrough curves, where van Leer (1974) provided the best interpretation of the upper end of the curve (Figure 10). The results of the sensitivity analysis of selected parameters are shown in Figure 12 - each case differs from the "original prediction" by only one investigated parameter.

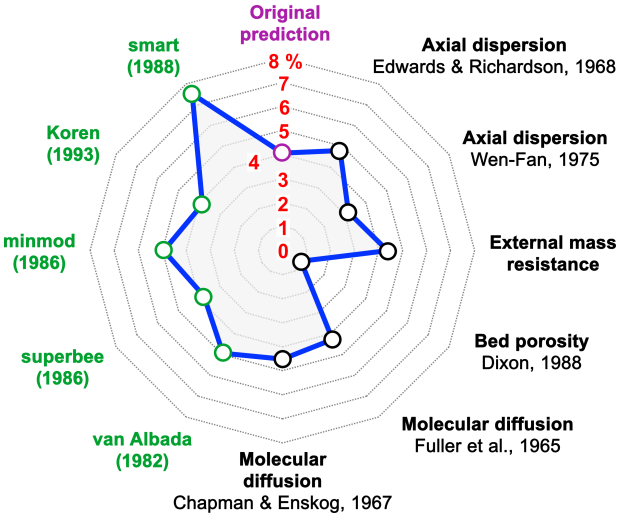

FIGURE 12. A deviation from the breakthrough curve onset time at 293 K and 2 bar. *Note:* Correlations were taken from [28, 34, 36, 41, 51–55].

4. CONCLUSIONS

Two sets of breakthrough experiments were performed at 2 and 5 bar at different temperatures in the laboratory adsorption apparatus, each for 5 cycles. The reported breakthrough curves showed no significant deviation between the cycles at each adsorption temperature, which established a solid ground for the simulation studies. The most prominent feature was the reduction of influence of the adsorption temperature on the amount adsorbed at 5 bar. Hence we can conclude that high-pressure system could provide a solution for processing wet gas stream by adsorbing CO_2 at elevated temperatures, above the dew point of the flue gas, without substantially lowering the amount adsorbed - a further research will be conducted in

this manner. Zeolite 13X possessed a high adsorption capacity at low pressures and temperatures below 293 K, while adsorption at high pressures did not provide significant advantages. The highest adsorption capacity of 0.1313 $\mathrm{g_{CO_2}}/\mathrm{g_{dry\ adsorbent}}$ was measured at 283 K and 5 bar and 0.1188 $\mathrm{g_{CO_2}}/\mathrm{g_{dry\ adsorbent}}$ at 283 K and 2 bar.

A quick assessment of the parameter optimisation makes the simulation a powerful tool that can save time, space, and financial funds once properly tuned with respect to the experiment. It was particularly evident for the breakthrough onset time, where the deviation did not exceed 2 % from the averaged experimental value. The prediction of the breakthrough curve tail, where the outlet CO_2 concentration reaches its plateau, yielded lower accuracy. A possible cause could be the assumption of isothermal conditions, which, in some studies, shortened the time of reaching the plateau of the breakthrough curve (i.e., steepened the breakthrough curve tail). Depending on the temperature rise during the adsorption, this effect appears to be more prominent and will be investigated further. Therefore, this area was not easy to investigate by the sensitivity analysis, which was therefore performed for the breakthrough onset time. The main conclusions can be summarised as follows:

- Column geometry, adsorption temperature and pressure, and volumetric flow are the easiest way to regulate adsorption time, by reducing or postponing the breakthrough onset time.
- The investigated parameters had a mild impact on the breakthrough onset time of up to 3.6 % from the original prediction. The bed porosity, which is defined by the adsorbent particle size and shape, bed configuration, and the type of packing, affects the largest number of parameters, and should always be accounted for.
- Non-linear numerical schemes are preferable for modelling adsorption processes.

Acknowledgements

This work was supported by the project TK03030167 "Low-emission technologies of energy conversion of biomass and alternative fuels" by the Technology Agency of the Czech Republic (TACR), which is gratefully acknowledged.

List of symbols

b, b_0 Langmuir equilibrium constant $[\mathrm{m^3/mol}]$
Bi Biot number [–]
c Concentration in the gas phase $[\mathrm{mol/m^3}]$
d_p Adsorbent particle diameter [m]
d_{pore} Adsorbent pore diameter [m]
D_{ax} Axial dispersion coefficient $[\mathrm{m^2/s}]$
D_{in} Bed inner diameter [m]
D_{eff} Effective diffusion coefficient $[\mathrm{m^2/s}]$
$D_K = \left(y_{CO_2}/D_{K,CO_2} + y_{N_2}/D_{K,N_2}\right)^{-1}$ Overall Knudsen diffusion $[\mathrm{m^2/s}]$
D_M Molecular diffusion coefficient $[\mathrm{m^2/s}]$
k Mass transfer rate [1/s]
$k_f = (\mathrm{Sh}\cdot D_{M,\,CO_2-N_2})/d_p$ External mass transfer rate [1/s]
L Length [m]
m_m Material weight [kg]
M Molar weight [mol/kg]
P Pressure [Pa, bar]
$\mathrm{Pe}_\infty = 6.7 d_p$ Péclet number (limiting value) [–]
r_p Particle diameter [m]
$R = 8.314$ Universal gas constant $[\mathrm{J/(mol\,K)}]$
$\mathrm{Re_p} = \rho_g\, u_0\, d_p/\mu_g$ Reynolds number for particle [–]
q Concentration in the solid phase $[\mathrm{mol/m^3}$, mol/kg]
q^* Adsorbed amount at equilibrium $\left[\mathrm{mol/m^3},\ \mathrm{g_{CO_2}}/\mathrm{g_{dry\ adsorbent}}\right]$
S_{BET} BET surface area $[\mathrm{m^2/kg}]$
Sh Sherwood number [–]
t Time [s]
t_w Column wall thickness, [m]
$u = u_0/\varepsilon_b$ Interstitial velocity [m/s]
u_0 Superficial velocity [m/s]
ΔU Internal adsorption energy [J/mol]
V_{flow} Volumetric flow $[\mathrm{dm^3/min}]$
V_m Material volume, Fig.1 $[\mathrm{m^3}]$
V_p Particle volume $[\mathrm{mm^3}]$
V_{pore} Pore volume $[\mathrm{m^3/kg}]$
$y_i = c_i/c$ Dimensionless concentration in the gas phase [–]
z Axial coordinate of the column [–]

β, γ Coefficients, Eq. 2 [–]
ε_b Bed porosity [–]
ε_p Particle porosity [–]
μ_g Gas dynamic viscosity [Pa S]
ν Molar volume of gas $[\mathrm{m^3/mol}]$
$\pi_1 = (u_0\,\varepsilon_p\, d_p^2\,\varepsilon_b)/[4\,L_{col}\,D_{eff}\,(1-\varepsilon_b)]$ $\Pi - 1$ factor [–]
π_2 $\Pi - 2$ factor [–]
ρ_g Gas density $[\mathrm{kg/m^3}]$
$\rho_p = \rho_b/(\varepsilon_b - 1)$ Particle density $[\mathrm{kg/m^3}]$
τ Tortuosity [–]

0^+ Position right after the column inlet
0^- Position right before the column inlet
$_{13X}$ Adsorbent bed of zeolite 13X
$_{col}$ Column
$_{emp}$ Empty space
$_{gb}$ Inert material (glass beads), Tab 1
$_i$ i-th component
$_{in}$ Column inlet
$_m$ Material
$_p$ Particle
$_{sat}$ State of adsorbent saturation
$_w$ Column wall

References

[1] D. Coe, W. Fabinski, G. Wiegleb. The Impact of CO2, H2O and Other "Greenhouse Gases" on Equilibrium

Earth Temperatures, *International Journal of Atmospheric and Oceanic Sciences* **5**(2):29-40, 2021. https://doi.org/10.11648/j.ijaos.20210502.12.

[2] M. Menner, G. Reichert. *EU Climate Policy in Light of the Corona Crisis*. cepInput. No. 18, 2020. https://www.cep.eu/fileadmin/user_upload/cep.eu/Studien/cepInput_Klima_und_Corona/cepInput_EU_Climate_Policy_in_Light_of_the_Corona_Crisis_01.pdf.

[3] S. E. Zanco, J.-F. Pérez-Calvo, A. Gasós, et al. Postcombustion CO2 Capture: A Comparative Techno-Economic Assessment of Three Technologies Using a Solvent, an Adsorbent, and a Membrane. *ACS Engineering Au* **1**(1):50-72, 2021. https://doi.org/10.1021/acsengineeringau.1c00002.

[4] M. M. F. Hasan, R. C. Baliban, J. A. Elia, et al. Modeling, Simulation, and Optimization of Postcombustion CO2 Capture for Variable Feed Concentration and Flow Rate. 1. Chemical Absorption and Membrane Processes. *Industrial & Engineering Chemistry Research* **51**(48):15642-64, 2012. https://doi.org/10.1021/ie301571d.

[5] M. M. F. Hasan, R. C. Baliban, J. A. Elia, et al. Modeling, Simulation, and Optimization of Postcombustion CO2 Capture for Variable Feed Concentration and Flow Rate. 2. Pressure Swing Adsorption and Vacuum Swing Adsorption Processes. *Industrial & Engineering Chemistry Research* **51**(48):15665-82, 2012. https://doi.org/10.1021/ie301572n.

[6] C. Song, Q. Liu, N. Ji, et al. Alternative pathways for efficient CO2 capture by hybrid processes - A review. *Renewable and Sustainable Energy Reviews* **82**:215-31, 2018. https://doi.org/10.1016/j.rser.2017.09.040.

[7] T. Zarogiannis, A. I. Papadopoulos, P. Seferlis. Systematic selection of amine mixtures as post-combustion CO2 capture solvent candidates. *Journal of Cleaner Production* **136**:159-75, 2016. https://doi.org/10.1016/j.jclepro.2016.04.110.

[8] M. Sheng, S. Dong, Z. Qiao, et al. Large-scale preparation of multilayer composite membranes for post-combustion CO2 capture. *Journal of Membrane Science* **636**, 2021. https://doi.org/10.1016/j.memsci.2021.119595.

[9] N. Fouladi, M. A. Makarem, M. A. Sedghamiz, et al. CO2 adsorption by swing technologies and challenges on industrialization. In *Advances in Carbon Capture*, p. 241-67. 2020. https://doi.org/10.1016/b978-0-12-819657-1.00011-6.

[10] C. Dhoke, A. Zaabout, S. Cloete, et al. Review on Reactor Configurations for Adsorption-Based CO2 Capture. *Industrial & Engineering Chemistry Research* **60**(10):3779-98, 2021. https://doi.org/10.1021/acs.iecr.0c04547.

[11] F. Raganati, R. Chirone, P. Ammendola. CO2 Capture by Temperature Swing Adsorption: Working Capacity As Affected by Temperature and CO2 Partial Pressure. *Industrial & Engineering Chemistry Research* **59**(8):3593-605, 2020. https://doi.org/10.1021/acs.iecr.9b04901.

[12] K. N. Son, T.-M. J. Richardson, G. E. Cmarik. Equilibrium Adsorption Isotherms for H2O on Zeolite 13X. *Journal of Chemical & Engineering Data* **64**(3):1063-71, 2019. https://doi.org/10.1021/acs.jced.8b00961.

[13] F. Raganati, F. Miccio, P. Ammendola. Adsorption of Carbon Dioxide for Post-combustion Capture: A Review. *Energy & Fuels* **35**(16):12845-68, 2021. https://doi.org/10.1021/acs.energyfuels.1c01618.

[14] D. Danaci, M. Bui, N. Mac Dowell, et al. Exploring the limits of adsorption-based CO2 capture using MOFs with PVSA - from molecular design to process economics. *Molecular Systems Design & Engineering* **5**(1):212-31, 2020. https://doi.org/10.1039/c9me00102f.

[15] P. Ammendola, F. Raganati, R. Chirone, et al. Fixed bed adsorption as affected by thermodynamics and kinetics: Yellow tuff for CO2 capture. *Powder Technology* **373**:446-58, 2020. https://doi.org/10.1016/j.powtec.2020.06.075.

[16] D. Bahamon, A. Díaz-Márquez, P. Gamallo, et al. Energetic evaluation of swing adsorption processes for CO 2 capture in selected MOFs and zeolites: Effect of impurities. *Chemical Engineering Journal* **342**:458-73, 2018. https://doi.org/10.1016/j.cej.2018.02.094.

[17] A. A. Abd, S. Z. Naji, A. S. Hashim, et al. Carbon dioxide removal through physical adsorption using carbonaceous and non-carbonaceous adsorbents: A review. *Journal of Environmental Chemical Engineering* **8**(5), 2020. https://doi.org/10.1016/j.jece.2020.104142.

[18] J. A. A. Gibson, E. Mangano, E. Shiko, et al. Adsorption Materials and Processes for Carbon Capture from Gas-Fired Power Plants: AMPGas. *Industrial & Engineering Chemistry Research* **55**(13):3840-51, 2016. https://doi.org/10.1021/acs.iecr.5b05015.

[19] M. Xu, S. Chen, D.-K. Seo, et al. Evaluation and optimization of VPSA processes with nanostructured zeolite NaX for post-combustion CO2 capture. *Chemical Engineering Journal* **371**:693-705, 2019. https://doi.org/10.1016/j.cej.2019.03.275.

[20] D. Sachde, R. McKaskle, J. Lundeen, et al. Review of Technical Challenges, Risks, Path Forward, and Economics of Offshore CO2 Transportation and Infrastructure. *Offshore Technology Conference, Houston, Texas, USA, 6 - 9 May 2019*, 2019. https://doi.org/10.4043/29253-MS.

[21] S. G. Subraveti, S. Roussanaly, R. Anantharaman, et al. Techno-economic assessment of optimised vacuum swing adsorption for post-combustion CO2 capture from steam-methane reformer flue gas. *Separation and Purification Technology* **256**, 2021. https://doi.org/10.1016/j.seppur.2020.117832.

[22] M. Nait Amar, H. Ouaer, M. Abdelfetah Ghriga. Robust smart schemes for modeling carbon dioxide uptake in metal-organic frameworks. *Fuel* **311**, 2022. https://doi.org/10.1016/j.fuel.2021.122545.

[23] A. H. Farmahini, S. Krishnamurthy, D. Friedrich, et al. Performance-Based Screening of Porous Materials for Carbon Capture. *Chemical Reviews* **121**(17):10666-741, 2021. https://doi.org/10.1021/acs.chemrev.0c01266.

[24] S. Li, S. Deng, L. Zhao, et al. Mathematical modeling and numerical investigation of carbon capture by adsorption: Literature review and case study. *Applied Energy* **221**:437-49, 2018. https://doi.org/10.1016/j.apenergy.2018.03.093.

[25] B. Miklová, M. Staf, V. Kyselová. Influence of ash composition on high temperature CO2 sorption. *Journal of Environmental Chemical Engineering* **7**(2), 2019. https://doi.org/10.1016/j.jece.2019.103017.

[26] J. Zhang, P. Xiao, G. Li, et al. Effect of flue gas impurities on CO2 capture performance from flue gas at coal-fired power stations by vacuum swing adsorption. *Energy Procedia* **1**(1):1115-22, 2009. https://doi.org/10.1016/j.egypro.2009.01.147.

[27] P. Xiao, J. Zhang, P. Webley, et al. Capture of CO2 from flue gas streams with zeolite 13X by vacuum-pressure swing adsorption. *Adsorption* **14**(4-5):575-82, 2008. https://doi.org/10.1007/s10450-008-9128-7 .

[28] B. E. Poling, J. M. Prausnitz, J. P. O'Connell. *The Properties of Gases and Liquids, 5th ed.* McGraw-Hill Education, 768 p, 2001. ISBN 9780071499996.

[29] M. S. Shafeeyan, W. M. A. Wan Daud, A. Shamiri. A review of mathematical modeling of fixed-bed columns for carbon dioxide adsorption. *Chemical Engineering Research and Design* **92**(5):961-88, 2014. https://doi.org/10.1016/j.cherd.2013.08.018.

[30] N. S. Wilkins, A. Rajendran, S. Farooq. Dynamic column breakthrough experiments for measurement of adsorption equilibrium and kinetics *Adsorption* **27**(3):397-422, 2020. https://doi.org/10.1007/s10450-020-00269-6.

[31] A. Malek, S. Farooq, M. N. Rathor, et al. Effect of velocity variation due to adsorption-desorption on equilibrium data from breakthrough experiments. *Chemical Engineering Science* **50**(4):737-40, 1995. https://doi.org/10.1016/0009-2509(94)00245-m.

[32] A. Ribeiro, P. Neto, C. Pinho. Mean porosity and pressure drop measurements in packed beds of monosized spheres: side wall effects. *International Review of Chemical Engineering*, **2**(1):40-46, 2010.

[33] J. M. P. Q. Delgado. Longitudinal and Transverse Dispersion in Porous Media. *Chemical Engineering Research and Design* **85**(9):1245-52, 2007. https://doi.org/10.1205/cherd07017.

[34] G. Langer, A. Roethe, K. P. Roethe, et al. Heat and mass transfer in packed beds-III. Axial mass dispersion. *International Journal of Heat and Mass Transfer* **21**(6):751-9, 1978. https://doi.org/10.1016/0017-9310(78)90037-6.

[35] E. Glueckauf, J. I. Coates. 241. Theory of chromatography. Part IV. The influence of incomplete equilibrium on the front boundary of chromatograms and on the effectiveness of separation. *Journal of the Chemical Society (Resumed)*, 1947. https://doi.org/10.1039/jr9470001315.

[36] D. M. Ruthven, M. F. M. Post. Chapter 12 Diffusion in zeolite molecular sieves. In *Introduction to Zeolite Science and Practice*, Studies in Surface Science and Catalysis, p. 525-77. 2001. https://doi.org/10.1016/s0167-2991(01)80254-8.

[37] K. Ciahotný, A. Vagenknechtová, M. Netušil, et al. Adsorption Drying of Natural Gas Under High Pressure. *Oil Gas European Magazine*, **40**(2):91-95, 2014.

[38] X. Hu, E. Mangano, D. Friedrich, et al. Diffusion mechanism of CO2 in 13X zeolite beads. *Adsorption* **20**(1):121-35, 2013. https://doi.org/10.1007/s10450-013-9554-z.

[39] S. Krishnamurthy, R. Blom, M. C. Ferrari, et al. Adsorption and diffusion of CO2 in CPO-27-Ni beads. *Adsorption* **26**(5):711-21, 2019. https://doi.org/10.1007/s10450-019-00162-x.

[40] P. V. Danckwerts. Continuous flow systems. *Chemical Engineering Science* **2**(1):1-13, 1953. https://doi.org/10.1016/0009-2509(53)80001-1.

[41] S. Javeed, S. Qamar, W. Ashraf, et al. Analysis and numerical investigation of two dynamic models for liquid chromatography. *Chemical Engineering Science* **90**:17-31, 2013. https://doi.org/10.1016/j.ces.2012.12.014.

[42] M. Thommes, K. Kaneko, A. V. Neimark, et al. Physisorption of gases, with special reference to the evaluation of surface area and pore size distribution (IUPAC Technical Report). *Pure and Applied Chemistry* **87**(9-10):1051-69, 2015. https://doi.org/10.1515/pac-2014-1117.

[43] M. Hefti, D. Marx, L. Joss, et al. Adsorption equilibrium of binary mixtures of carbon dioxide and nitrogen on zeolites ZSM-5 and 13X. *Microporous and Mesoporous Materials* **215**:215-28, 2015. https://doi.org/10.1016/j.micromeso.2015.05.044.

[44] D. W. Siderius, V. K. Shen, R. D. Johnson, et al. *NIST/ARPA-E Database of Novel and Emerging Adsorbent Materials*. National Institute of Standards and Technology, 2020. (Accessed 2022-05-06) https://doi.org/10.18434/T43882.

[45] K. N. Pai, V. Prasad, A. Rajendran. Practically Achievable Process Performance Limits for Pressure-Vacuum Swing Adsorption-Based Postcombustion CO2 Capture. *ACS Sustainable Chemistry & Engineering* **9**(10):3838-49, 2021. https://doi.org/10.1021/acssuschemeng.0c08933.

[46] H. Bekhti, H. Bouchafaa, R. Melouki, et al. Adsorption of CO2 over MgO-Impregnated NaY zeolites and modeling study. *Microporous and Mesoporous Materials* **294**, 2020. https://doi.org/10.1016/j.micromeso.2019.109866.

[47] S. Sircar, R. Kumar, K. J. Anselmo. Effects of column nonisothermality or nonadiabaticity on the adsorption breakthrough curves. *Industrial & Engineering Chemistry Process Design and Development* **22**(1):10-5, 2002. https://doi.org/10.1021/i200020a002.

[48] B. Berdenova, A. Pal, B. B. Saha, et al. Non-isothermal pore change model predicting CO2 adsorption onto consolidated activated carbon. *International Journal of Heat and Mass Transfer* **177**, 2021. https://doi.org/10.1016/j.ijheatmasstransfer.2021.121480.

[49] P. Bollini, N. A. Brunelli, S. A. Didas, et al. Dynamics of CO2 Adsorption on Amine Adsorbents. 1. Impact of Heat Effects. *Industrial & Engineering Chemistry Research* **51**(46):15145-52, 2012. https://doi.org/10.1021/ie301790a.

[50] I. Roušar, P. Ditl. Numerical Simulation of Multicomponent Isobaric Adsorption in Fixed Bed Columns. *Adsorption Science & Technology* **3**(2):49-59, 1986. https://doi.org/10.1177/026361748600300201.

[51] J. M. P. Q. Delgado. A critical review of dispersion in packed beds. Heat and Mass Transfer, 2005, 42(4), 279-310, https://doi.org/10.1007/s00231-005-0019-0.

[52] A. G. Dixon. Correlations for wall and particle shape effects on fixed bed bulk voidage. *The Canadian Journal of Chemical Engineering* **66**(5):705-8, 1988. https://doi.org/10.1002/cjce.5450660501.

[53] N. Wakao, T. Funazkri. Effect of fluid dispersion coefficients on particle-to-fluid mass transfer coefficients in packed beds. *Chemical Engineering Science* **33**(10):1375-84, 1978. https://doi.org/10.1016/0009-2509(78)85120-3.

[54] Ch. Tien. *Introduction to Adsorption.* Elsevier (S&T), 2019. ISBN 978-0-12-816446-4.

[55] G. D. Silcox, J. J. Noble, A. F. Saforim et al. Heat & Mass Transfer. In: *Don W. Green, Marylee Z. Southard. Perry's Chemical Engineers' Handbook, 9th Edition.* McGraw-Hill Education, p. 510-583, 2019. ISBN 978-0-07-183409-4.